ZrW catalyzed cellulose conversion in hydrothermal conditions: Influence of the calcination temperature and insights on the nature of the active phase

?. van Chuc Nguyen, A. Dandach, ?. Thi Thu Ha Vu, P. Fongarland, N. Essayem

ZrW catalyzed cellulose conversion in hydrothermal conditions: Influence of the calcination temperature and insights on the nature of the active phase

Van Chuc NGUYEN[1,2], Amar DANDACH[1], Thi Thu Ha VU[2], Pascal FONGARLAND[1], Nadine ESSAYEM[1*]

[1]*Institut de Recherche sur la Catalyse et l'environnement de Lyon, CNRS, Lyon1, 2 Avenue Albert Einstein, 69626 Villeurbanne, France*

[2]*Key Laboratory for Petrochemical and Refinery Technologies, 2 rue Pham Ngu Lao, Hanoi, Vietnam*

* nadine.essayem@ircelyon.univ-lyon1.fr

Abstract

Tungstated zirconia, ZrW, is reported as an efficient solid acid catalyst in the conversion of cellulose into lactic acid in hydrothermal conditions. The active phase of ZrW is generally ascribed to more or less polymerized WO_x domains dispersed on zirconia. In this study, commercial uncalcined and calcined tungstated zirconia were used as catalysts for the conversion of cellulose under hydrothermal conditions at 190 °C. Their activities were also compared with uncalcined zirconium oxyhydroxide, $ZrO_{2-x}(OH)_{2x}$ and calcined zirconia, ZrO_2. Contrary to the expected results, it is disclosed that uncalcined ZrW exhibits higher catalytic activity and stability than calcined ZrW. Modifications in the products distribution were observed as glycolic acid formation at the expense of lactic acid formation upon ZrW calcination. Even more surprising, the catalytic activity of W free amorphous zirconium oxyhydroxide $ZrO_{2-x}(OH)_{2x}$ is similar to uncalcined ZrW, with lactic acid as the main product while ZrO_2 does not have any catalytic activity. These results suggest that the active phase of these catalysts might combine the couple Zr^{4+} and OH^- species while the role of W species would be of secondary importance.

Keyworks: cellulose liquefaction, tungstated zirconia, zirconium oxyhydroxide, lactic acid, glycolic acid

1. Introduction

Lignocellulosic biomass is a renewable carbon source. Generally, the lignocellulosic biomass contains 35–50 % of cellulose, 20–35 % of hemi-cellulose, and 10–25% of lignin. Cellulose, the major component of lignocellulosic biomass is a biopolymer composed of glucose units linked by β-1,4-glucosidic bonds. The linear chains of glucose units, linked via intermolecular and intramolecular hydrogen bonds, are packed into microfibrils. This structure is responsible for the difficult depolymerization of cellulose into chemicals and fuels under mild conditions, in conventional solvents. Some methods of cellulose depolymerization were developped, for example, depolymerisation of cellulose with enzyme [1,2], with liquid mineral acids [3,4], or hydrolysis in non-conventional solvents such as ionic liquids [5,6] and supercritical media [7,8]. Heterogeneous catalysts were also successfully used to promote cellulose depolymerisation under hydrothermal conditions [9-12].

Among the various cellulosic biomass derivatives, lactic acid is regarded as a high potential platform chemical manufactured in very large quantity for industrial applications and consumer products such as acrylic acid [13], propylene glycol [14], pyruvic acid [15] and (poly) lactides [16]. Currently, lactic acid is produced via fermentation processes of sugars which presents some drawbacks such as slow kinetics, complex purification, poor scalability, and large amounts of waste formation [17]. To overcome these drawbacks, various chemo-catalytic processes, implemented in water, have been studied as well using homogeneous or heterogeneous catalysts. Yan et al.[18] reported the production of 19 % yield of lactic acid using $Ca(OH)_2$ under subcritical water at 300 °C for 90 seconds. Zhang et al.[19] obtained lactic acid yield of 42 % at 300 °C, for 5 min in the presence of 0.02 g Zn, 0.03 g Ni, 0.07 g activated carbon and NaOH 2.5 mol/L. Wang et al.[20] found that $PbCl_2$ exhibited a remarkable promoting effect on cellulose conversion to lactic acid. A lactic acid yield of 68 % was obtained from ball-milled cellulose (33 % crystallinity) with Pb^{2+} at 190 °C for 4 h under 3 MPa N_2. Lei et al.[21] investigated the hydrothermal conversion of cellulose to lactic acid using $ErCl_3$. As a result, the highest lactic acid yield reported to date was 91 % at 240 °C for 30 min under 2 MPa N_2 using 0.1 g cellulose, 0.05 g $ErCl_3$ and 30 mL water. However, using homogeneous catalysts have the disadvantage of difficult catalysts recovery from the reaction mixtures, and thus limits their use in lactic acid

production. Besides, effective heterogeneous catalyst were also reported. In 2011, we reported lactic acid yields of 28 mol% and 19 mol% from microcrystalline cellulose over tungstated zirconia (ZrW) and tungstated alumina (AlW) respectively, at 190 °C for 24 h under 5 MPa He [22]. Yang et al.[23] reported a lactic acid yield of 24 % from cellulose using $LaCoO_3$ perovskite with redox properties and a good stability in hydrothermal media at 200 °C for 1 h. Hou et al.[24] used $Pb(OH)_2$/rGO to convert cellulose to lactic acid with the yield of 32 % at 190 °C, for 4 h under 2.5 MPa N_2. Lactic acid yields higher than 50% were recently reported over catalysts presented as heterogeneous ones: Wu et al.[25] reported a lactic acid yield of 58% using Er/Beta-zeolite at 240 °C for 30 min and Wang et al.[26] reported that 68 % yield of lactic acid can be obtained from cellulose with Er-exchanged montmorillonite K10 catalyst at 240 °C for 30 min. Most of researches generally consider that the activity of heterogeneous catalysts for lactic acid formation from cellulose to is due to Lewis acid -base properties or redox properties of solid materials. Note that the contribution of solubilized active species is not investigated in a systematic way. Moreover, comparison between published data is not easy due to the variability of important parameters such as the source of cellulose, eventually its preatreatment, the catalysts/cellulose ratio, water/cellulose ratio among the most important ones.

Tungstated zirconia (ZrW) is an efficient and environmentally benign solid acid catalyst. There are many studies on ZrW catalysts dealing with their preparation, characterization and acidic properties [27-30]. These catalysts exhibit excellent activity for various gas or liquid phase organic reactions. A major advantage of these catalysts is their relatively stability in a broad variety of temperature conditions as weel in gas or liquid phases. Reddy et al.[31] reported that ZrW was a effective catalyst for the acetylation of alcohols, phenols and amines with high yields of products (89-98%) within short reaction times (1-4 h). Sakthivel et al.[32] reported that WO_3/ZrO_2 with WO_3 content of 19 wt.% was the best catalyst for Friedel-Crafts acetylation of anisole with acetic anhydride to make 2- and 4-methoxy-acetophenone among a series of 5, 10, 15, 19 and 25 wt.% WO_3/ZrO_2. Bordoloi et al.[33] found that 15 wt.% WO_3/ZrO_2 calcined at 800°C was the most active for the acetylation of veratrole with acetic anhydride to produce 3,4-dimethoxy acetophenone and toluene alkylation with 1-dodecene. Ramu et al. [34] reported that WO_3/ZrO_2 with low WO_3 loading (5wt.% WO_3) shows maximum catalytic activity for esterification of palmitic acid with methanol among a series of WO_3/ZrO_2 catalysts containing from 2.5 to 25 wt.% WO_3. López et al.[35] investigated the effect of calcination temperature

(400–900°C) on the catalytic properties of ZrW with the goal of determining the optimum pretreatment temperature and increasing the understanding of the nature of the active sites for esterification of acetic acid and transesterification of triacetin. The catalyst calcined at 800°C exhibited the highest catalytic activity. In an earlier study, we had also investigated the influence of the calcination temperature of ZrW for dibenzothiophene oxidation with H_2O_2. It was demonstrated that the uncalcined solids containing tetrahedral WO_4^{2-} species show higher activity than clusters of WO_3 formed after calcination at 973K [36]. Usually, ZrW are calcined at high temperature for catalytic applications and there is a general agreement on the nature of the active phase of ZrW related to WO_x domains, from isolated tetra-coordinated WO_4^{2-} species up to W based isopolyanions more or less dispersed on the zirconia supports, depending on the W amount, on the method of synthesis and on the calcination temperature [35,37]. One must admit that there are as many ZrW as there are modes of synthesis.

Activity/structure correlations were obtained from gas phase or organic liquid catalytic applications. Applications of ZrW for aqueous phase transformations are rather limited and more recent since linked mainly with carbohydrates conversion [22,38]. In this study, we investigate the effect of calcination on the catalytic activity of ZrW for the conversion of cellulose into lactic acid in hydrothermal conditions. We also compared the catalytic activity of uncalcined and calcined ZrW with zirconium oxyhydroxide ($ZrO_{2-x}(OH)_{2x}$) and zirconia (ZrO_2). Our goal was to get deeper insights on the nature of the actives phase.

2. Experimental part

2.1. Materials

A model commercial cellulose, named "Native fibrous cellulose MN 301", standard grade, 95 % of fibers with length 2–20 µm, average degree of polymerization 400–500 from Macherey-Nagel, was used as model substrate for hydrolysis reaction.

Amorphous tungstated zirconium hydroxide, XZO1251 (15 wt% WO_3), was provided by MEL Chemicals (UK) and named uncalcined ZrW in the following.

Tungstated zirconia was prepared by calcination of amorphous tungstated zirconium hydroxide under air flow for 3 h, at 700°C, using a temperature ramp of 5°C/min, and named calcined ZrW.

Zirconium (IV) oxyhydroxide XZO1247, was provided by MEL Chemicals (UK) and named $ZrO_{2-x}(OH)_{2x}$.

Zirconium oxide was prepared by calcination of zirconium oxyhydroxide in identical conditions, under air flow for 3 h, at 700°C, using a temperature ramp of 5°C/min, and named ZrO_2.

2.2. Catalysts characterizations

Thermogravimetric analysis- Differential thermal analysis were done using a Setaram DTA-DTG apparatus. 30mg of the sample were weighed in a platinum holder and heated under air flow to 800°C with the heating ramp of 5°C/min.

Elemental analysis for tungsten was performed using Inductively Coupled Plasma Emission Spectroscopy (ICP-OES). ICP-OES analysis were carried out at IRCELYON using an ACTIVA spectrometer manufactured by Horiba JOBIN YVON. ZrW catalysts were mineralized using a mixture of acids (H_2SO_4 + HCl + HNO_3) and heated at 250-300°C. After mineralization, the liquids are injected on the ICP-OES apparatus using a peristaltic pump. The solution is then nebulized (with argon) and directed to the plasma flame. The specific emission lines enable the identification and quantification of the elements.

X-ray diffractograms were recorded on a diffractometer Bruker D8 Advance A25 equipped with a copper anode. Samples were analyzed within a range of 4 - 80 ° (2θ) with a step of 0.02 ° and with a measurement acquisition time of 96s per step. The analysis were made at ambient temperature and on powders.

Catalysts textures were studied by **N_2 adsorption-desorption isotherms**. BET surface areas (S_{BET}) were determined using a multipoint BET method. Before S_{BET} analysis, the catalyst samples were degassed at 150°C under 10^{-3} Torr for 3 h. Adsorption measurements were carried out using UHP N_2 adsorption-desorption at –196°C in a Micromeritics ASAP 2020 device.

TEM images were obtained with a JEOL 2010 microscope. The acceleration voltage was 200 kV with LaB6 emission current and the resolution was 0.19 nm. Before measurements, a dispersion of crushed catalyst in ethanol was deposited on standard holey carbon-covered copper TEM grids.

The Raman spectra of uncalcined and calcined ZrW samples were obtained at room temperature in ambiant atmosphere. Raman measurements were carried out in a Jobin-Yvon LabRam Infinity

apparatus equipped with a CCD detector with laser source (λ = 520 nm). The Raman spectra were recorded in the range 0–3500 cm^{-1}.

XPS measurements were performed using a Kratos Axis Ultra DLD spectrometer. Spectra of W4s, Zr3d, O1s levels were measured at 90° (normal angle with respect to the plane of the surface) using a monochromated Al K X-ray source with an excitation energy of 1486.6 eV. The signal intensities of W4s, Zr3d, O1s were measured using integrated areas under the detected peak.

The acidic strength of the solids was characterized by NH_3 adsorption at 80 °C, using **a TianCalvet calorimeter** coupled with a volumetric ramp. The samples (0.02 g), placed in the glass cell, were first pre-treated at 150ºC, for 4 h under secondary vacuum, then placed into the calorimeter up to the stabilization of the temperature (one night), then contacted with successive small doses of gas while the differential enthalpies of adsorption were recorded.

FTIR-pyridine spectra of self-supported pellets of the sample were recorded with a Brucker Vector 22 spectrometer in the absorption mode with a resolution of 2 cm^{-1}. The samples were placed in an IR glass cell equipped with KBr windows and treated in situ. The wafer of all samples was pretreated at 150ºC under secondary vacuum for 2h. Pyridine was adsorbed under saturated vapor pressure at ambient temperature then desorbed at 150ºC for 30min (after 30 min of temperature increase under vacuum) in order to remove the physisorbed pyridine species.

2.3. Catalytic tests

The reaction conditions are as follows: the cellulose (MN301, 1.6 g), the catalyst (0.68 g) and water (65 mL) were introduced in a 100mL Paar Hastelloy autoclave equipped with a Rushton turbine under autogeneous pressure at 190ºC. The autoclave was purged with He and heated. The starting time is the time when the temperature reached 190°C (~after 25 min). For the kinetic study, the reactor was stopped and cooled rapidly in ice bath after different set times.

All reaction products in liquid phase were analyzed by HPLC with an ICE COREGEL 107H column (300mm×7.8mm, 40°C) and a refractive index detector using acidified water as eluent (0.6 mL/min, 0.005 mol% H_2SO_4).

The total mass of carbon in the liquid phase (=the solubility of cellulose in water) was analyzed by a Shimadzu TOC-VSCH total organic carbon (TOC) analyzer (720 ◦C, Pt/Al_2O_3 catalyst, IR detector):

$$\text{Solubility (\%)} = 100 \times \frac{\text{mg C}_{\text{liquid phase}}}{\text{mg C}_{\text{initial cellulose}}}$$

The conversion of cellulose was calculated as the ratio of the cellulose consumption in the reaction and the initial cellulose. The unconverted cellulose in solid residue after reaction was measured by quantitative FTIR [39].

$$\text{Conversion (\%)} = 100 \times \left(1 - \frac{m_{\text{unconverted cellulose}}}{m_{\text{initial cellulose}}}\right)$$

The carbon yields of the products, determined by HPLC, were calculated as the molar ratio of the product i and the initial glucosyl units present in the initial cellulose, corrected by the number of carbon atoms:

$$\text{yield}_i\ (C\%) = 100 \times \left(\frac{nC_i}{6}\right) \times \left(\frac{n_i}{nC_{\text{glucose unit}}}\right)$$

nC_i: number of carbon atoms in the product i; n_i: number of moles of the product i determined by the HPLC analysis; $n_{\text{glucosyl units}}$: initial number of moles of glucosyl units in the cellulose sample $=m_{\text{cellulose}}/162$.

The yield of soluble oligosaccharides and polymers (SOP) was deduced from the difference between the solubility of cellulose analyzed by TOC and sum of the carbon yields of products analyzed by HPLC:

$$\text{yield}_{SOP}\ (\%) = \text{solubility (\%)} - \Sigma\text{yield}_i\ (\%)$$

The yield of solid residue was deduced from the difference between the conversion of cellulose analyzed by IR and the solubility of cellulose:

$$\text{yield}_{\text{solid residue}}\ (\%) = \text{conversion (\%)} - \text{solubility (\%)}$$

The distribution of soluble oligosaccharides in the liquid phase and the depolymerization progress of the cellulose were determined by High-Performance Anion-Exchange Chromatog-

raphy equipped with Pulsed Amperometric Detection (PAD). The apparatus used was a Dionex ICS 3000 chromatograph. An amperometric detector is composed of a minicell voltammetry which produces the oxidation of secondary hydroxyl functions of sugars on a gold electrode (Potential +0.10 V). The separation was performed on a CarboPac PA1 column, using as eluent, a mixture of water, sodium hydroxide (300 mmol L−1 isocratic) and sodium acetate (300 mmol L−1) with the total flow of 1 mL min−1. Under these conditions, simple sugars (glucose, galactose, fructose, manose are eluted at the same retention time, rt ~2.5 min, while the retention times of oligosaccharides, progressively increase with their number of glucose units (cellobiose (rt=5.6 min) , cellotriose (rt=7.8 min), etc.

3. Results and discussion

3.1. Effect of calcination on WZr features

Thermogravimetric analysis of the uncalcined ZrW in air showed a total weight loss of about 13% (Fig. 1). These weight losses observed at T<500°C results from a loss of physisorbed and structural water. No further weight loss occurred from 500 to 800 °C. Elemental analysis showed that tungsten contents in uncalcined ZrW and calcined ZrW at 700ºC are 11.6 and 12.0% (Table 1). The weight loss of $ZrO_{2-x}(OH)_{2x}$ at 500ºC is about 24% from the thermogravimetric analysis. The higher total weight loss of $ZrO_{2-x}(OH)_{2x}$ than that of uncalcined ZrW can be mainly explained by the release of the higher amount of physisorbed water from the surface of $ZrO_{2-x}(OH)_{2x}$ at the temperature less than 200ºC. However, a higher amount of water loss due to dehydroxylation at temperatures between 200 and 500°C is also observed on $ZrO_{2-x}(OH)_{2x}$ by comparison to uncalcined ZrW. The main exothermic peak, observed at 445°C over $ZrO_{2-x}(OH)_{2x}$ is shifted at higher temperature over ZrW. This modification of the temperature of cristallisation of the zirconia phase, shifted at higher temperature in the presence WO_x oxoxanions, was already observed [36].

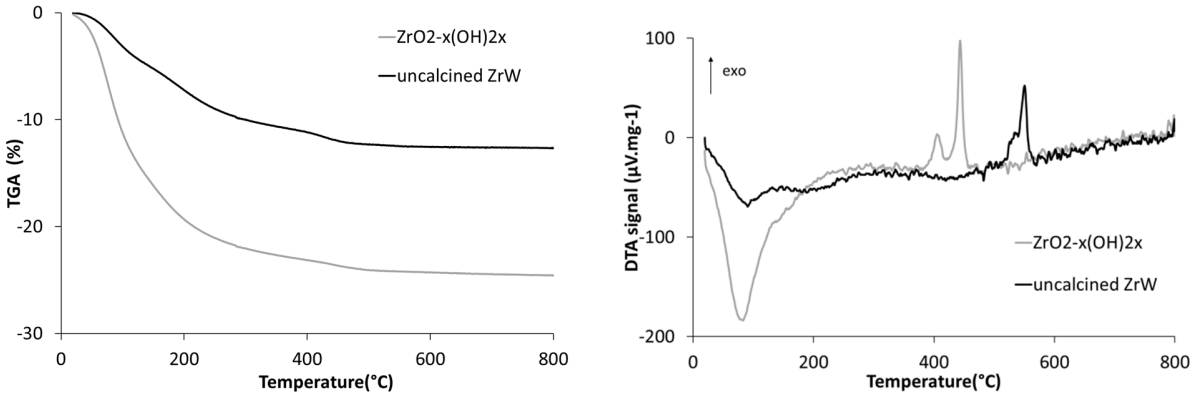

(a) **(b)**

Figure 1. ***TGA-DTA curves of uncalcined ZrW and $ZrO_{2-x}(OH)_{2x}$ under air flow***

a)Thermogravimetric analysis, b) Differential thermal analysis

The effect of calcination on the phase formation was also observed using XRD (Fig. 2). Both un-calcined ZrW and $ZrO_{2-x}(OH)_{2x}$ are amorphous. After $ZrO_{2-x}(OH)_{2x}$ calcination at 700°C, W free ZrO_2 is mainly composed of monoclinic phase with a little amount of tetragonal phase, while calcined ZrW is mostly composed of tetragonal phase. The phase transformation of ZrO_2 is changed with the loading of WO_x oxoanions on $ZrO_{2-x}(OH)_{2x}$. With pure zirconium oxyhydroxide, it is known that the metastable tetragonal phase occurs at 350°C and then is transformed to monoclinic phase at 470°C [40,41,42]. This is in good agreement with the XRD pattern observed after calcination of the zirconium oxyhydroxide at 700°C, the main phase of ZrO_2 is the monoclinic one. After loading WO_x oxoanions, the tetragonal phase of ZrO_2 is stabilized at moderate calcination temperatures (500–800°C) [35,43]. All these phenomenona are already well reported in the literature. The results of DTA analysis confirm that the phase transition of ZrO_2 in un-calcined ZrW occurred at higher temperature than $ZrO_{2-x}(OH)_{2x}$, still in good agreement with the literature data [36] (Fig 1-b). In uncalcined and calcined ZrW patterns, no WO_3 diffraction peaks are observed suggesting an optimal dispersion of WO_x species within the zirconia support. From the TEM-EDX analysis, it is confirmed that W is well dispersed before and after calcination, without observation of WO_x clusters with diameter higher than 1 nm (Fig. 3).

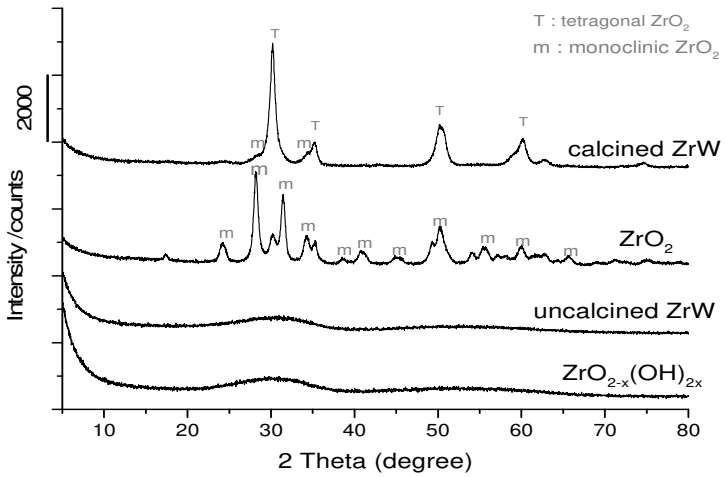

Figure 2*: The XRD patterns of ZrO_2-x$(OH)_{2x}$ and ZrW before and after calcination*

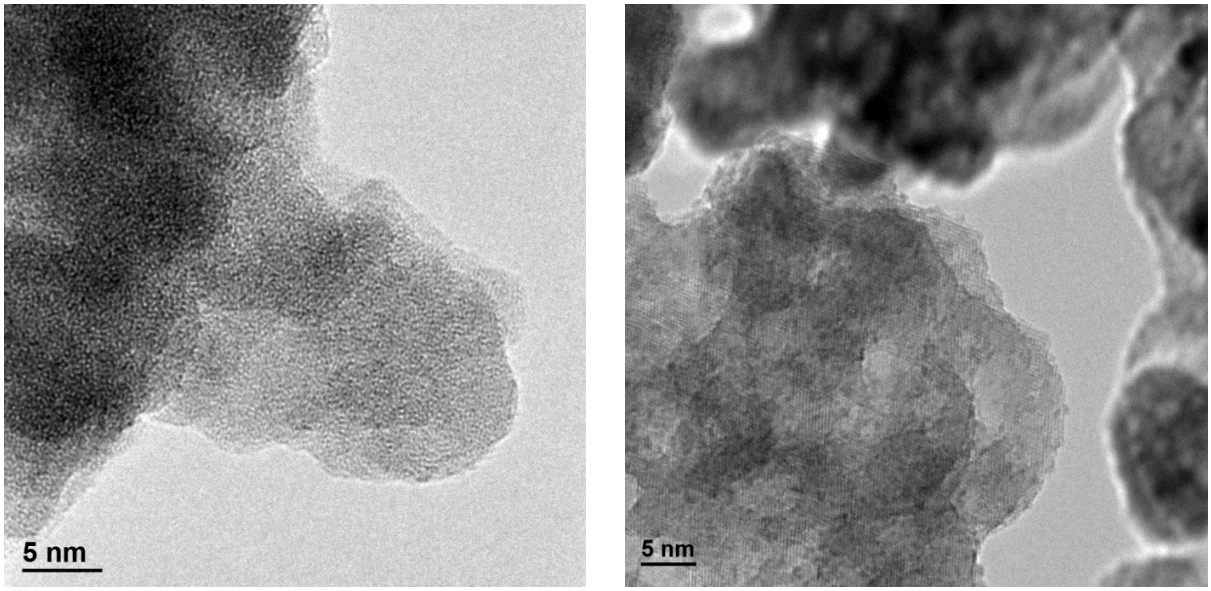

(a) **(b)**

Figure 3*. TEM images of a) uncalcined ZrW and b) calcined ZrW*

The surface area of $ZrO_{2-x}(OH)_{2x}$ and un-calcined ZrW are significantly decreased after calcination (Table 1). The surface area of un-calcined ZrW was about 345 $m^2.g^{-1}$, slightly lower than that of $ZrO_{2-x}(OH)_{2x}$ (401 $m^2.g^{-1}$). After calcination of the W free oxyhydroxide at 700°C, the formed ZrO_2 has a surface area of 39 $m^2.g^{-1}$ only. This is a result of the densification of ZrO_2 structure that also involves the formation of the monoclinic phase. The surface area of calcined ZrW was 107m^2/g, higher than that of W free ZrO_2. This was previously ascribed to WO_x oxoanions which stabilize the porous structure of ZrO_2 [43], by preventing the formation of large ZrO_2 crystallites in agreement with the XRD patterns of calcined ZrW with broad diffraction peaks of ZrO_2 tetragonal phase.

Table 1. ***Surface area, chemical analysis and acidic properties of catalysts***

Catalyst	**un-calcined ZrW**	**Calcined ZrW**	$ZrO_{2-x}(OH)_{2x}$	**ZrO_2**
W (wt%)	11.6	12.0	-	-
BET Surface area ($m^2.g^{-1}$)	345	107	401	39
Total acid sites number(mmole.g^{-1}) *	0.68	0.27	0.39	0.06

** determined by microcalorimetry: total acid sites with differential heat of NH_3 adsorption >80kJ.mol^{-1}.*

FTIR spectra of the four samples are shown on Fig. 4. The absorption band centered at 3430 cm^{-1} is assigned to the $\nu_{(O-H)}$ stretching vibration of physically absorbed water molecules on the surface and/or to hydroxyl groups. The infrared absorption band at 1634 cm^{-1} is assigned to the bending vibration of adsorbed water molecules. These bands are the main ones on un-calcined ZrW and $ZrO_{2-x}(OH)_{2x}$ FTIR spectra and were strongly reduced after calcination. The thin infrared band at 1384 cm^{-1} may be due to nitrates from the Zr precursor. After calcination, it would decompose completely, and the infrared absorption band at 1384 cm^{-1} disappeared accordingly. New bands appeared at 730, 500 cm^{-1} on the ZrO_2 spectrum following the calcination of $ZrO_{2-x}(OH)_{2x}$ at 700 °C. The bands were previously ascribed to Zr–O–Zr stretching frequency of ZrO_2 [42,44]. The weak absorption bands around 936 cm^{-1} and 950 cm^{-1} for un-calcined and calcined ZrW respectively are attributed to the $\nu_{(WO)}$ stretching vibration[7]. As

already proposed [37], the blue shift of the $\nu_{(WO)}$ vibration upon calcination could indicate a change of the structure of W species, this might suggest that the supported WO_x species are more aggregated and /or that the interaction with the support is weaker.

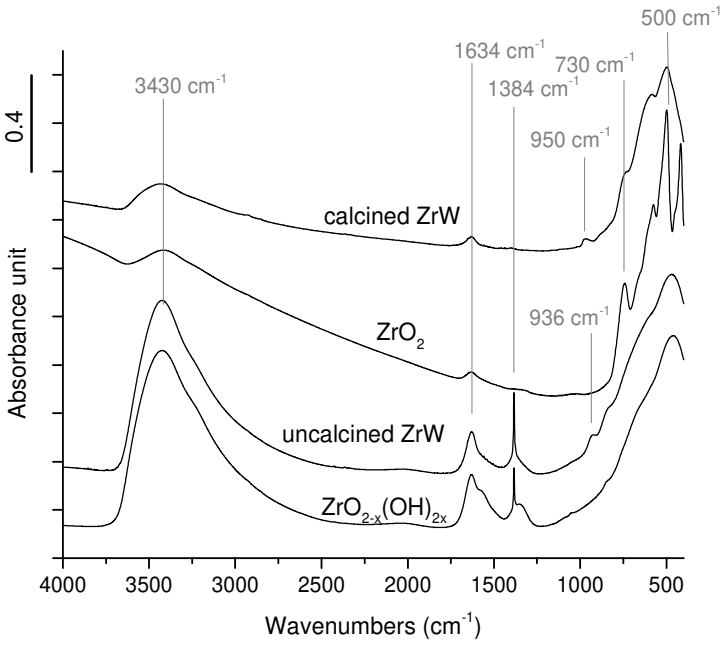

Figure 4. ***FT-IR spectra of*** $ZrO_{2-x}(OH)_{2x}$ ***and ZrW before and after calcination at*** *700°C.*

The chemical states of zirconium, tungsten and oxygen in uncalcined and calcined ZrW were analyzed by XPS (Fig. 5). After calcination at 700°C, the photopeaks Zr3d and W4f do not change, while the photopeak O1s is strongly modified: upon calcination the component at 531.5eV, ascribed to superficial hydroxyl groups, is strongly reduced as expected and in good agreement with data from the IR spectra.

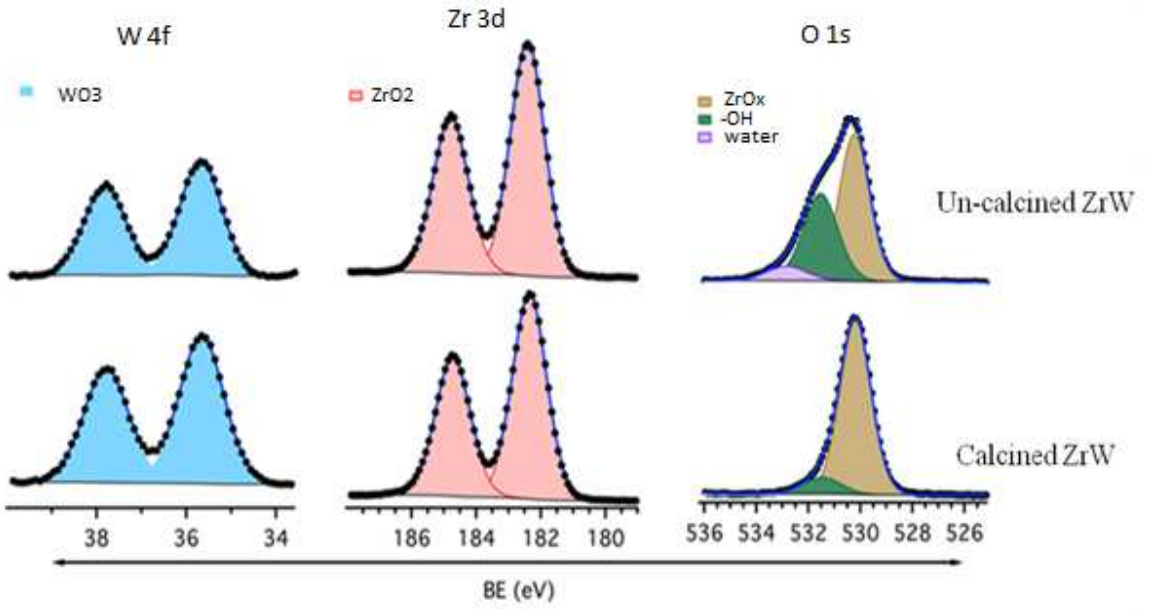

Figure 5. ***XPS spectra of uncalcined and calcined ZrW***

Raman spectroscopy was used to identify, at the molecular level, structural changes in the uncalcined and calcined ZrW samples (Fig. 6). The spectrum of uncalcined ZrW presents a main band at 930 cm^{-1} with a shoulder at 840 cm^{-1} already observed on uncalcined tungstated zirconia, prepared by anionic exchange [37]. These bands were previously ascribed to νs and νas vibrations of monomeric $(WO_4)^{2-}$ in tetrahedral symmetry. The two other bands, the sharp one at 1053 cm^{-1} and the broad one at 545 cm^{-1}, were already observed over zirconium hydroxide and assigned to the vibrations modes of carbonates and to $\nu_{(Zr\text{-}OH)}$ vibration respectively [37]. This is in good agreement with their disappearance upon calcination at 700°C. Besides, the spectra of calcined ZrW is completely different with the appearance of new bands such as the intense one at 645 cm^{-1} due to the formation of the tetragonal zirconia phase [35,43] and the $\nu_{(WO)}$ strechting vibration observed at higher frequencies, 980cm^{-1}. This suggests a structure evolution of the tungsten species during the crystallization of the tetragonal zirconia phase, probably a change of their coordination associated to their slight aggregation [35,45,37]. These evolutions probably occur together with a decrease of the interaction of the W species with the support which influences also the frequencies of the $\nu_{(WO)}$ vibration. This is consistent with the FTIR spectra reported above which show that the $\nu_{(WO)}$ vibration at 936 cm^{-1} was blue-shifted after calcination.

The two other broad bands observed at 880 an 830 cm^{-1} on the Raman spectra of the calcined ZrW were previously proposed to be due to $\nu_{(W\text{-}O\text{-}W)}$ and $\nu_{(W\text{-}O\text{-}Zr)}$ strentching vibrations.

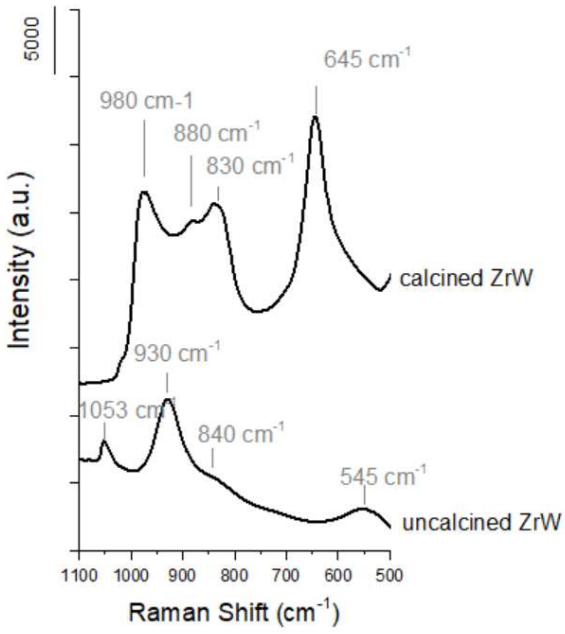

Figure 6. ***Raman spectra of uncalcined and calcined ZrW***

The acidity of the samples was characterized by both microcalorimetry of NH_3 adsorption (Fig. 7, Table1) and FTIR of pyridine adsorption (Fig. 8). From the microcalorimetry measurements, it is seen that the number and strength of the acid sites are higher in uncalcined ZrW and calcined ZrW by comparison to $ZrO_{2-x}(OH)_{2x}$ and ZrO_2, respectively. The following ranking in term of total acid sites was obtained uncalcined ZrW> $ZrO_{2-x}(OH)_{2x}$ > calcined ZrW>ZrO_2. Fig. 7 compares the FTIR spectra of pyridine adsorption over the four materials normalized by the same weigth of self supported pellet. The bands around 1540 cm^{-1}, typical of pyridinium ions, are observed on calcined/uncalcined ZrW and on the zirconium oxyhydroxide. The characteristic vibrations of pyridine coordinated to Lewis acid sites are observed at 1443 cm^{-1} and around 1608 cm^{-1} over the four materials. Note that the overall more intense absorptions bands of the adsorbed pyridine species are observed on uncalcined ZrW while the weakest intensity is seen over ZrO_2. This is in good agreement with the results of calorimetry of NH_3 adsorption.

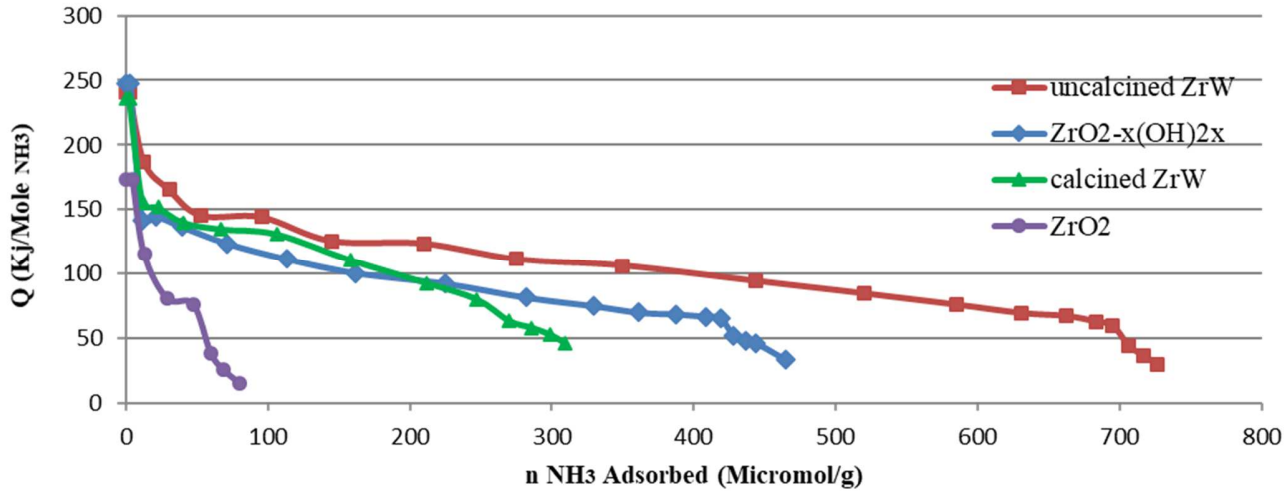

Figure 7. ***Microcalorimetry curves of samples***

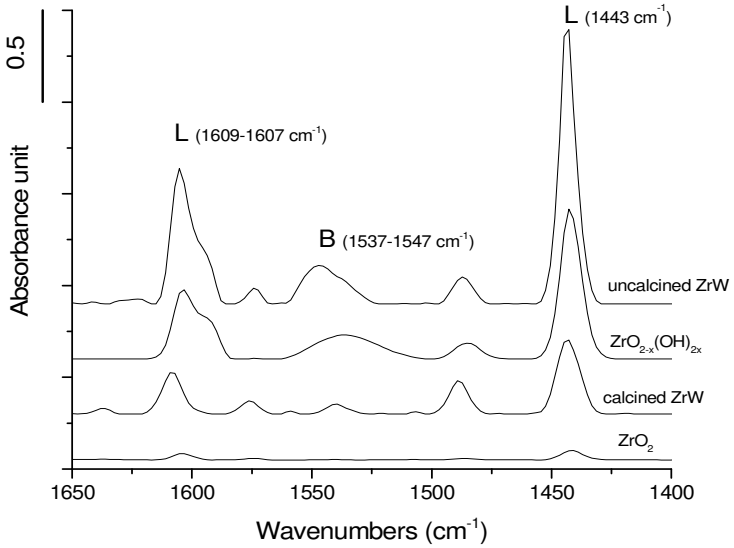

Figure 8. ***Room temperature spectra of pyridine (2kPa) adsorbed at room temperature and desorbed 1h at 150°C***

3.2. Hydrolysis of cellulose to lactic acid catalyzed by Zr containing materails

Let us first recall that the temperature of 190°C was chosen as reaction temperature because in one of our earlier study, it was shown that in water, the hydrolysis of microcrystalline cellulose occurs in water at T≥160°C, in the absence of any catalyst [46]. The solubility of microcrystalline cellulose in water was increased with the temperature: 35% of crystalline cellulose can be dissolved at 190 °C after 24 h of reaction. Since these earlier studies, we have completed the available analytic tools with FTIR analysis of unconverted cellulose [39]. As reported in the experimental part, it is now possible to discriminate between the cellulose conversion (from FTIR) from the cellulose solubility (from TOC). The kinetic of hydrolysis of the model cellulose selected in this study, "Native" fiber cellulose from Nagel Macherel, in the absence of catalyst, was shown in Fig. 3-9a. The cellulose solubility (TOC), which corresponds to soluble polymers and products eluted by HPLC, achieved 38% after 24h. This value is in agreement with the data earlier reported [46]. The quantification of the solid products along the reaction course deserves to be highlighted. Their proportion was significantly increased after 6h of reaction and represent 1/3 of the products after 24h. We observe also the parallel evolution of the soluble polymers which represents also 1/3 of the products after 24h. The main valuable products in the liquid reaction mixture are glucose, HMF and furfural. From 0h to 12h, the yields of these major products increase with the reaction time. However, for longer reaction time, their yields decrease with the appearance of levulinic acid. This indicates that their formation follows the usual Brønsted acid mechanism, in which, cellulose is depolymerized into soluble oligosaccharides and glucose, then dehydrated into HMF and further rehydrated into levulinic and formic acids, with the catalytic role of H_3O^+ produced by water self-protolysis (Scheme 1a). The conversion of cellulose does not acheive a plateau, the soluble polymers and solid products continuously increase with reaction time. The conversion of cellulose reaches 63% after 24h.

Then, the kinetic of cellulose hydrolysis in water was studied in the presence of uncalcined ZrW as catalyst (Fig. 9b). By comparison to the hydrolysis performed in absence of solid catalyst, the rate of cellulose transformation increases upon the addition of ZrW. The conversion of cellulose reaches 97% after 24h, a higher value than that obtained in absence of solid catalyst (64%). One can observe that the total liquid products detected by HPLC were also increased from a yield of 20% to 30% at the end of the reaction upon uncalcined ZrW addition. Furthermore, the liquid products distribution changes with lactic acid as the main product generally ascribed to the role

of Lewis acid sites in ZrW [22]. This consolidates the mechanism changes upon Lewis solid acid addition as proposed in Scheme 1b.

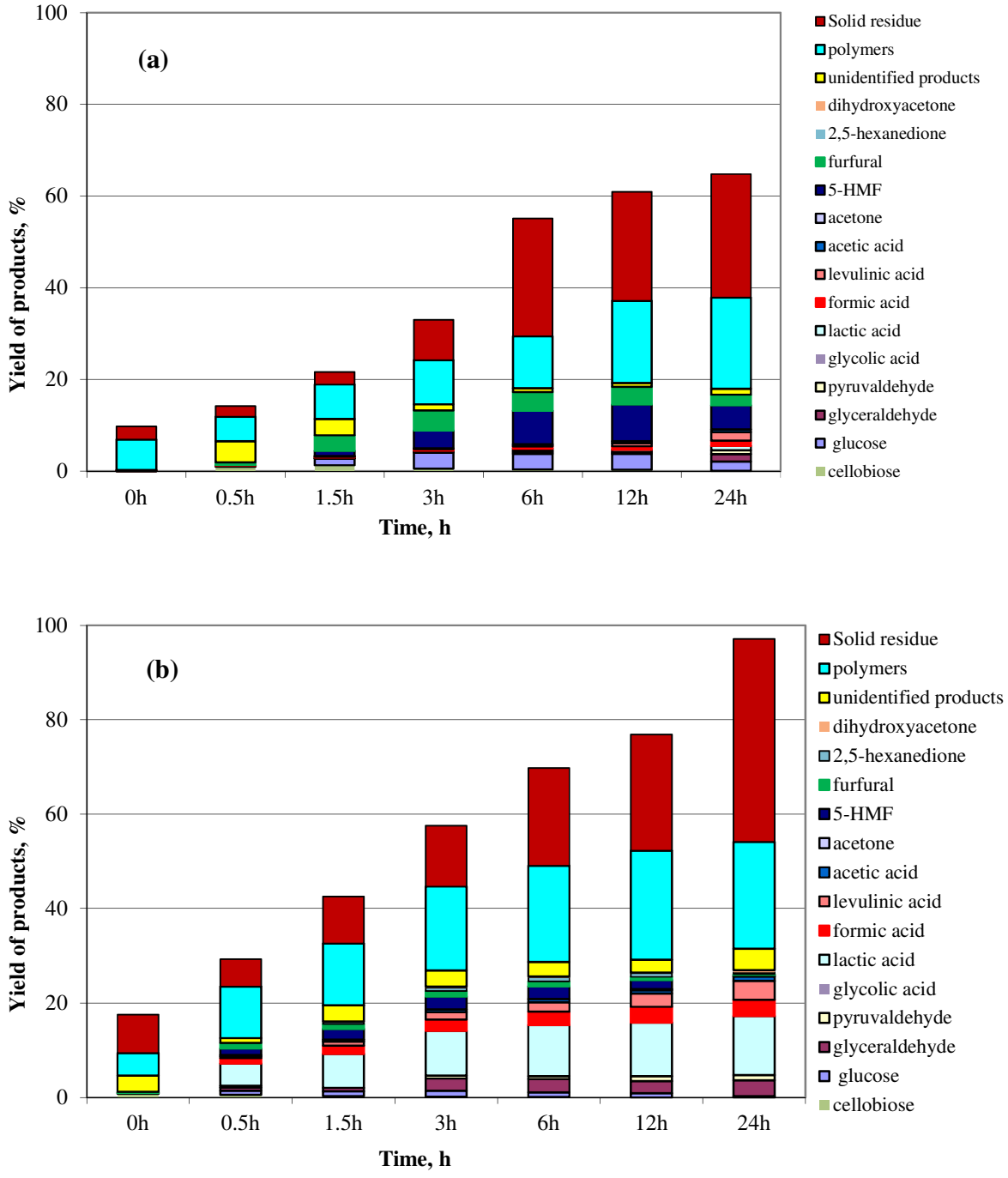

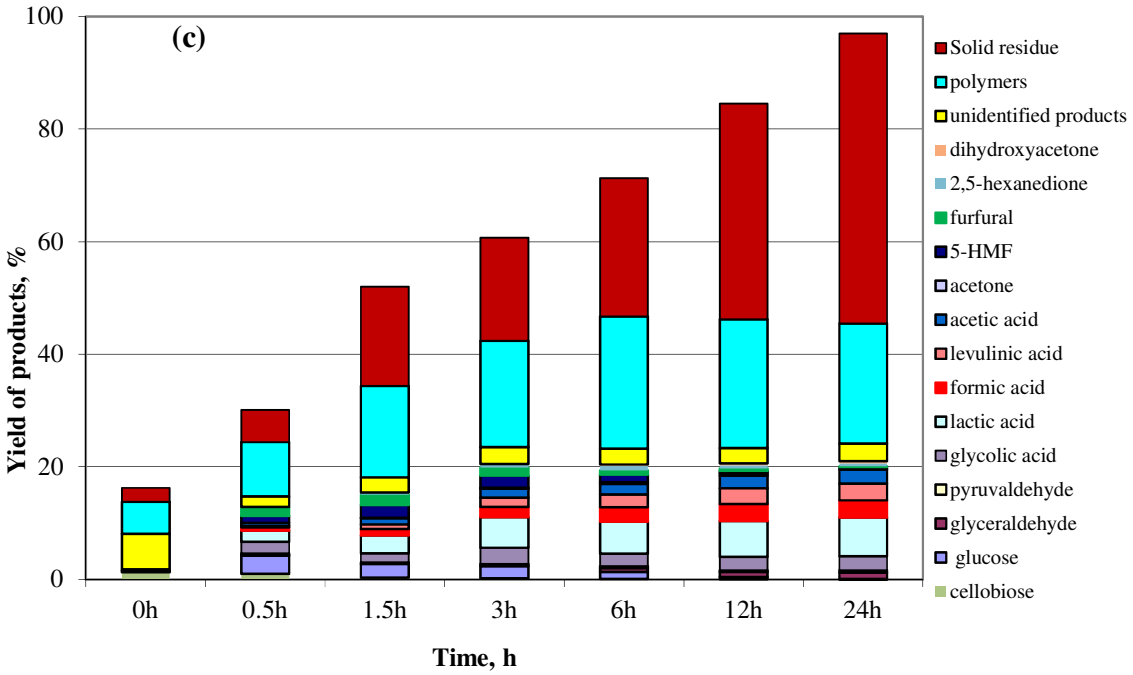

Figure 9. ***Kinetic of hydrolysis of cellulose (a) in absence of added catalyst (b) with un-calcined ZrW (c) with calcined ZrW***

T=190°C, ptot~11atm, $m_{catalyst}$= 0,68g, $m_{cellulose}$= 1,6g, m H_2O=65g, Ar purge

The latic acid yield increases continuously from the beginning period until 12% after 24h. Other organic acids such as formic acid and levulinic acid follows the same trend of lactic acid. The yields of soluble polymers and solid products also increase with reaction time. After 6h, the apparent solubility of cellulose is stable (soluble polymers + products analyzed by HPLC), while the conversion of cellulose still increases to produce much more solid residue.

Otherwise, the results of cellulose conversion using calcined ZrW was shown in Fig. 9c. The conversion and the rate of cellulose consumption are similar to un-calcined ZrW. The conversion of cellulose reaches to 96% after 24h. However, the liquid products distribution changes by comparison to uncalcined ZrW with a lower lactic acid yield (7% after 24h) balanced by higher yields of acetic acid and the appearance of glycolic acid. The yields of lactic acid and glycolic acid increase in parallel at the beginning period, reache nearly a plateau after 3h and keeps stable to 24h. Unlike lactic acid and glycolic acid, the yields of formic acid, levulinic acid, acetic acid still increase up to 24h. Note that the yields of soluble polymers also increase with reaction time

while the apparent solubility of cellulose is stable after 6h. Accordingly, the conversion of cellulose still increases to produce much more solid residue. The appearance of glycolic acid and acetic acid at the expense of lactic acid might be correlated to subtile changes in the superficial properties of the materials such as the otherall Lewis acidity but also the hydroxide groups which might intervene in the coordination of saccharides at the catalyst surface. The Lewis acidity is proposed to be the driving force to promote a chain mechanism involving successive elementary steps such as OH^- abstractions, hydride shift, α, β scissions who can account for the observed carboxylic acid formation (Scheme 1c).

To understand the role of the zirconium based supports on the conversion of cellulose, $ZrO_{2-x}(OH)_{2x}$ and ZrO_2 (obtained after $ZrO_{2-x}(OH)_{2x}$ calcination at 700°C) were used for cellulose hydrolysis under the same conditions (Fig. 10). To our surprise, the distribution and yield of the liquid products using $ZrO_{2-x}(OH)_{2x}$ are closed to that obtained with un-calcined ZrW. The main product is lactic acid, with an initial yield reaching nearly a plateau after 3h and leading to a yield of 11% after 24h. The yields in formic acid and levulinic acid increase also with the reaction time. The yield of HMF increases at the beginning period, and then, decreases to form levulinic acid. These results show that $ZrO_{2-x}(OH)_{2x}$ is a active phase for the conversion of cellulose to lactic acid in hydrothermal conditions, WO_x species supported on un-calcined zirconium oxyhydroxide would has a small role, most likely limited to the improvement of total Lewis acid site amounts. In the W free zirconium oxyhydroxide, it can be suggested that Zr^{4+}ions would act as the active Lewis acid sites. Most likely, the OH groups on the catalyst surface might favor the adsorption of the carbohydrate via hydrogen bonding resulting in the promotion of the conversion of cellulose into lactic acid.

By contrast to $ZrO_{2-x}(OH)_{2x}$, the results of cellulose conversion using ZrO_2 are different to the calcined ZrW. The lower yields of lactic acid and glycolic acid are tentatively correlated to the lower Lewis acid sites amount and the lower hydroxyls group density. Moreover, the distribution of liquid products is similar with the one observed in the absence of catalyst. The main products in the liquid reaction mixture are glucose, HMF and furfural. This products distribution shows that the reaction is carried out under the driving force of Brønsted acid sites provided from water self-protolysis with a very limiting effect of the few amounts of Lewis acid sites of ZrO_2.

To check if the observed results are only dependent on the surface area of the catalysts, 6.8 g of ZrO_2 (representing a total specific surface area of 265 m^2) was used in the reaction to reach the similar surface area of 0.68 g of $ZrO_{2-x}(OH)_{2x}$ (s_{BET}=273 m^2). The results showed that the yields of the main products such as lactic acid and formic acid using ZrO_2 are still lower than that using $ZrO_{2-x}(OH)_{2x}$. This suggests that the superficial OH groups of the Zr support play most likely a key role in the conversion of cellulose into lactic acid.

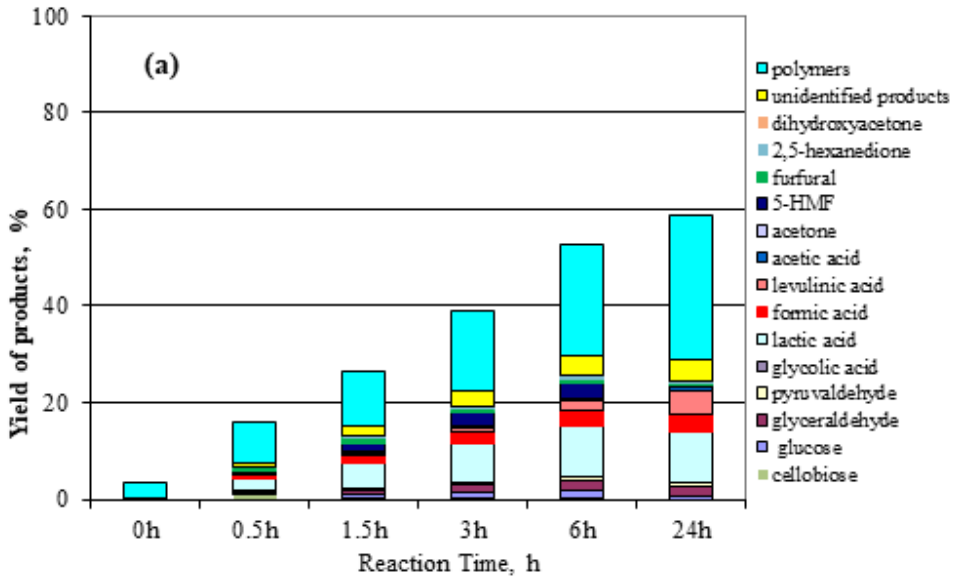

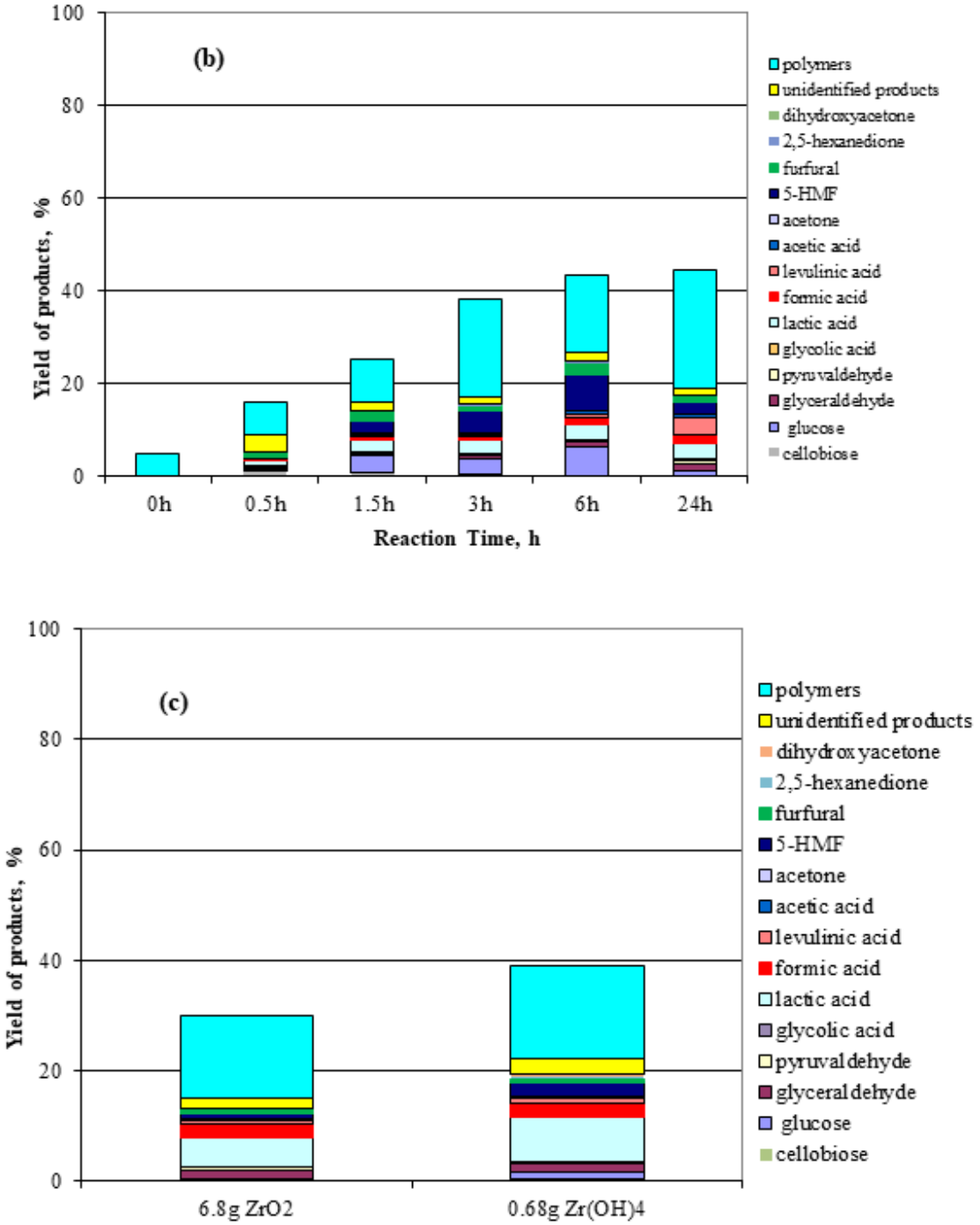

Figure 10. Kinetic of hydrolysis of cellulose with (a) $ZrO_{2-x}(OH)_{2x}$ and (b) ZrO_2 and (c) the catalytic activity comparation of ZrO_2 and $ZrO_{2-x}(OH)_{2x}$ at the similar surface area

T=190°C, p~11at, t=3h, $m_{cellulose}$= 1,6g, m H_2O=65g, Ar purge

The differences in the nature of the produced oligosaccharides during the course of the reaction were investigated by IC-PDA (Fig. 11). Let us recall that with this chromatographic technic, simple sugars (glucose, galactose, fructose, manose are eluted at the same retention time, rt ~2.5 min, while the retention times of oligosaccharides, progressively increase with their number of glucose units (cellobiose (rt=5.6 min) , cellotriose (rt=7.8 min), etc... At 0h (once the reaction media reached the set T of 190°C), oligosaccharides with more than 3 glucose units *(detected at retention > 7.8 min)* are detected in the liquid mixture in the presence of un-calcined and calcined ZrW as well (Fig. 11a-b). After 1.5h, there are no more oligosaccharides with more than 3 glucoses units in the liquid mixture. However, the proportion of oligossacharides derivatives with 2 or 3 glucose units *(with 5 min<rt< 8 min)* is more important over uncalcined ZrW compared to calcined ZrW. This accounts most likely for subtle changes in the mechanism between the two catalysts.

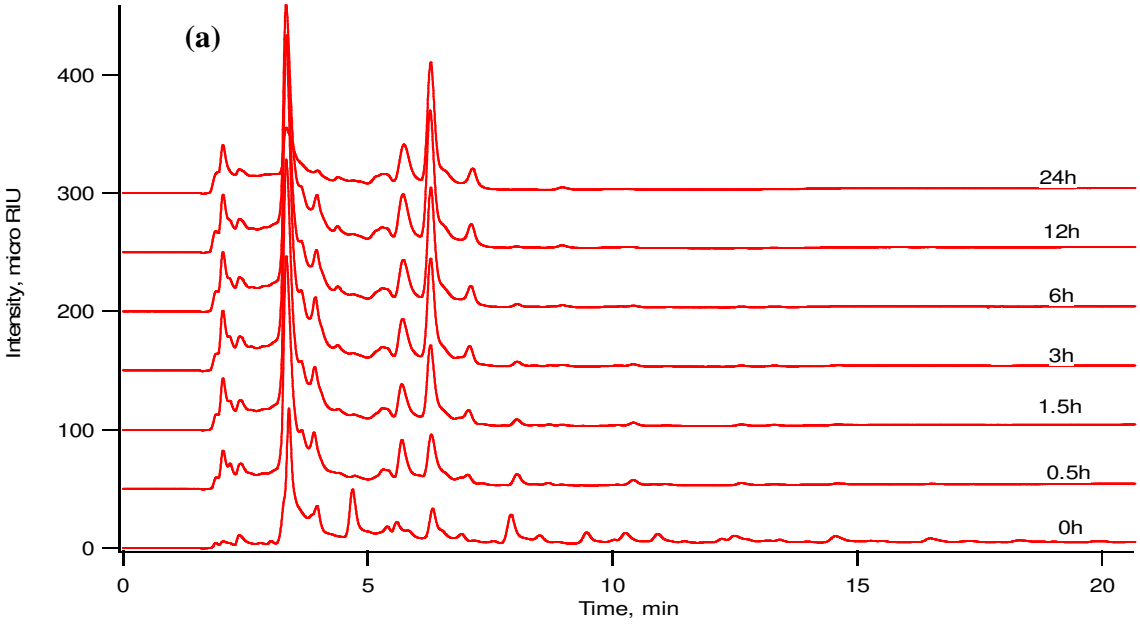

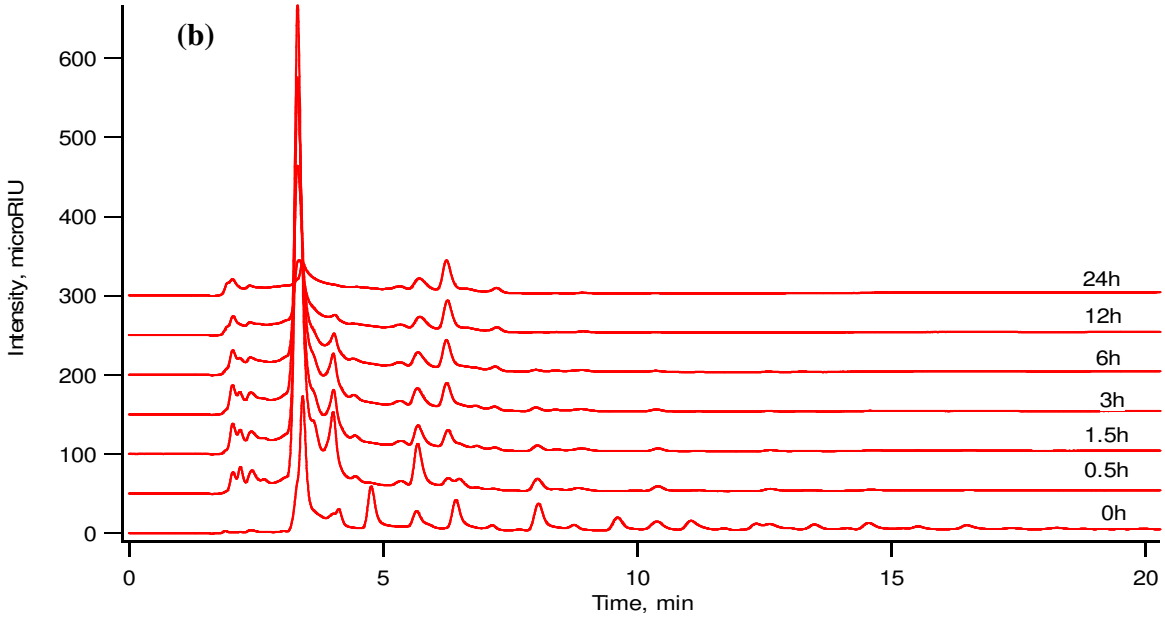

Figure 11. ***Oligosaccharides analysis of liquid mixtures (a) with un-calcined ZrW, (b) calcined ZrW***

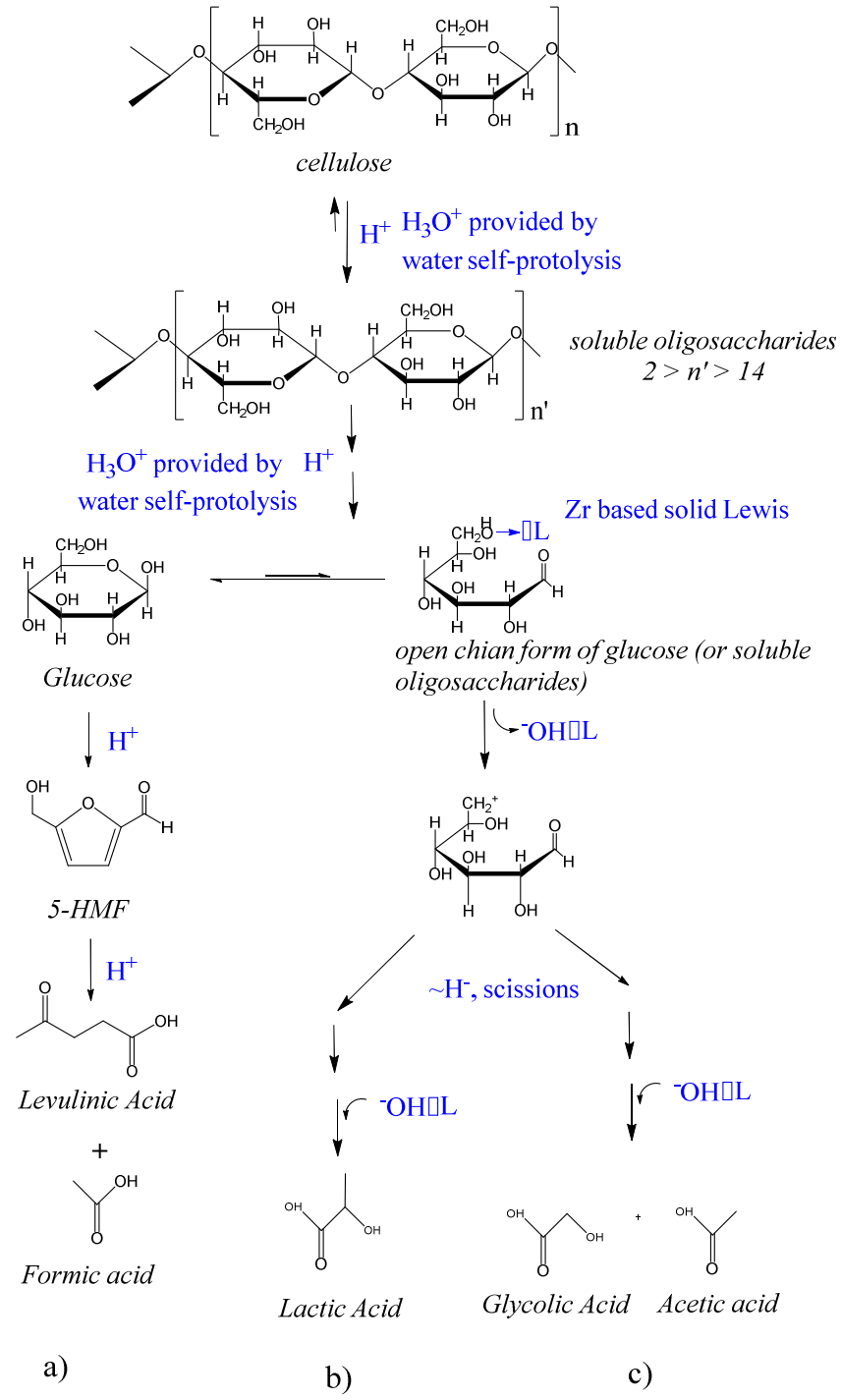

Scheme 1: Proposed main mechanism pathways for cellulose hydrolysis into carboxylic acids a) in catalysts free conditions b) in presence of uncalcined ZrW or Zr oxyhydroxide c) in presence of calcined ZrW

The leaching of catalysts elements was controlled by measuring the concentration of metallic ions in the liquid reaction mixture by ICP (Table 2). For both catalysts, calcined or un-calcined ZrW, there is no leaching of Zr after 24h. To our surprise, the leaching of W in un-calcined ZrW is significantly smaller than that of calcined ZrW. Over calcined ZrW, the W leaching progressively increases up to 1.5% after 24h of reaction while over uncalcined ZrW, leached W remains lower than 0.1% of the W content. This shows that un-calcined ZrW is more stable than calcined ZrW in hydrothermal conditions. Let us recall, that this is in complete contradiction with the known impact of calcination on the catalysts stability established for catalysts implemented in gas phase or in less polar, liquid organic media. The higher W leaching in calcined ZrW may be caused by the presence of more aggregated tungsten species as deduced from the Raman spectra. These species would be less strongly anchored on the ZrO_2 surface by comparision to uncalcined ZrW which contents highly dispersed tetrahedral $(WO_4)^{2-}$ entities.

Table 2. ***Zr and W leaching from catalysts as a function of reaction timess***

Time , (h)	**Leaching of uncalcined ZrW**		**Leaching of calcined ZrW**	
	% Zr	**% W**	**% Zr**	**% W**
0	~ 0	0	~ 0	0,5
0.5	~ 0	0.04	~ 0	1,2
1.5	~ 0	0.04	~ 0	1,5
3	~ 0	0.06	~ 0	1,6
6	~ 0	0.07	~ 0	1,7
12	~ 0	0,06	~ 0	1,5
24	~ 0	0,04	~ 0	1,5

Conclusions

We have shown that the total number and strength of acid sites of uncalcined and calcined ZrW are higher than the corresponding supports $ZrO_{2-x}(OH)_{2x}$ and ZrO_2. The Lewis acidity is dominant whatever the material is calcined or not. The calcination affects strongly the density of OH groups without significant changes in the nature acidity, i.e. the Lewis acidity is not favored at the expense of Brønsted ones. The reaction mechanism of cellulose hydrolysis changes upon addition of uncalcined or calcined ZrW but also upon $ZrO_{2-x}(OH)_{2x}$ addition as regards to the catalyst free conditions. By contrast, calcined ZrO_2 does not change the cellulose hydrolysis as regards to the solid catalyst free conditions. The distribution of the main reaction products shifted from HMF and levulinic acid formation in the absence of catalyst to lactic acid, glycolic acid with the presence of uncalcined/calcined ZrW or $ZrO_{2-x}(OH)_{2x}$. A lower yield of lactic acid is observed with calcined ZrW by comparison to uncalcined ZrW. This is balanced by the formation of glycolic acid. The distribution and yield of the liquid products obtained over $ZrO_{2-x}(OH)_{2x}$ are very close to uncalcined ZrW with equivalent lactic acid yield as the main product. By contrast, ZrO_2 is not efficient to produce Lactic acid. This unexpected result underlines the probable role of the couple Zr^{4+} and OH^- groups to drive efficiently the cellulose conversion into Lactic acid. In uncalcined ZrW and $ZrO_{2-x}(OH)_{2x}$, we propose that the active phase for the conversion of cellulose to lactic acid is composed of Lewis acid sites based on Zr^{4+} in close proximity with hydroxide groups OH^-.The role of W species, as monomeric tetrahedral $(WO_4)^{2-}$ entities in uncalcined ZrW, would be of secondary importance and would contribute to strengthen the acid strength and to increase the amout of acid sites as observed by calorimetry. The presence of slightly agglomerated WOx species in calcined ZrW would provide differenciated acid sites responsible for glycolic acid formation, a product observed over uncalcined ZrW exclusively. Moreover, in this work, a result of primary importance was obtained in the field of catalysts design for biomass processing in water: **uncalcined ZrW is more stable than calcined** ZrW in the hydrothermal conditions.

Acknowledgements

The authors gratefully acknowledge the financial supports from the Project Management Unit of FIRST for this sub-project through grant agreement No. 06/FIRST/2A/KEYLABPRT.

The authors also acknowledge the scientific services of IRCELYON for performing XRD, XPS, ICP, TEM analysis and Marion Ethernot for IC-PDA analysis of oligosaccharides.

References

[1] H. Pala, M. Mota, F. M. Gama, Carbohydrate Polymers 68 (2007) 101–108.

[2] H. Niu, N. Shah, C. Kontoravdi, Biochemical Engineering Journal 105 (2016) 455–472.

[3] K.J. Dussán, D.D.V. Silva, E.J.C. Moraes , P.V. Arruda , M.G.A. Felipe, Chemical Engineering Transactions 38 (2014) 433-438.

[4] F. Camacho, P. Gonzalez-Tello, E. Jurado, A. Robles, J. Chem. Tech. Biotechnol. 67 (1996) 350-356.

[5] S. Morales-delaRosa, J.M. Campos-Martin, J.L.G. Fierro, Chemical Engineering Journal 181–182 (2012) 538–541.

[6] Y. Xiong, Z. Zhang, X. Wang, B. Liu, J. Lin, Chemical Engineering Journal 235 (2014) 349–355.

[7] M. Sasaki, B. Kabyemela, R. Malaluan, S. Hirose, N. Takeda, T. Adschiri, K. Arai, Journal of Supercritical Fluids 13 (1998) 261–268.

[8] Y. Zhao, W-J. Lu, H-T. Wang, Chemical Engineering Journal 150 (2009) 411–417.

[9] L. Hu, Z. Li, Z. Wu, L. Lin, S. Zhou, Industrial Crops and Products 84 (2016) 408–417.

[10] L. Hu, L. Lin, Z. Wu, S. Zhou, S. Liu, Applied Catalysis B: Environmental 175 (2015) 225–243.

[11] L. Negahdar, I. Delidovich, R. Palkovits, Applied Catalysis B: Environmental 184 (2016)

285–298.

[12] S. Xu, M-C Liao, H-Y Zeng, C-R Chen, H-Z Duan, X-J Liu, J-Z Du, Applied Clay Science 115 (2015) 124–131.

[13] J. Zhang, J. Lin, P. Cen, Can. J. Chem. Eng. 86 (2008) 1047-1053.

[14] A. Primo, P. Concepción, A. Corma, Chem. Commun, 47 (2011) 3613–3615.

[15] M. Ai, Applied Catalysis A: General 23 (2002) 235–243.

[16] P. Delgado, M. T. Sanz, S. Beltrán, L. Alberto Nunez, Chemical Engineering Journal 165

(2010) 693–700.

[17] F. A. Castillo Martinez, E. M. Balciunas, J. M. Salgado, J. M. Domínguez González, A. Converti, R. Pinheiro de Souza Oliveira, Trends in Food Science & Technology, 30 (2013) ,70-83.

[18] X. Yan, F. Jin, K. Tohji, A. Kishita, H. Enomoto, AIChE Journal, 56 (10) (2010) 2727–2733.

[19] S. Zhang, F. Jin, J. Hu, Z. Huo, Bioresour Technol, 102(2) (2011) 1998–2003.

[20] Y. Wang, W. Deng, B. Wang, Q. Zhang, X. Wan, Z. Tang, Y. Wang, C. Zhu, Z. Cao, G.

Wang, H. Wan, Nat. Commun. 4, (2013) 2141–2148.

[21] X. Lei, F-F. Wang, C-L. Liu, R-Z. Yang, W-S. Dong, Applied Catalysis A: General 482 (2014) 78–83.

[22] F. Chambon, F. Rataboul, C. Pinel, A. Cabiac, E. Guillon, N. Essayem, Applied Catalysis

B: Environmental 105 (2011) 171–181.

[23] X. Yang, L. Yang, W. Fan, H. Lin, Catalysis Today, 269 (2016) 56–64.

[24] G-H. Hou, L-F Yan, Chin. J. Chem. Phys., 28(4) (2015) 533-538.

[25] H-Z. Wu, F-F. Wang, H-F. Ren, C-L. Liu, C-L. Xu, W-S. Dong, Journal of Porous Materials, 24 (3) (2017) 697-697.

[26] F-F. Wang, J. Liu, H. Li, C-L. Liu, R-Z. Yang, W-S. Dong, Green Chem., 17 (2015) 2455–2463.

[27] P. Wongmaneenil, B. Jongsomjit, P. Praserthdam, Journal of Industrial and Engineering Chemistry 16 (2010) 327–333.

[28] R. Kourieh, S. Bennici, A. Auroux, J Therm Anal Calorim 99 (2010) 849–853.

[29] G. Rodriguez-Gattorno, A. Galano, E. Torres-García, Appl. Catal., B:Environmental 92 (2009) 1-8.

[30] V.V. Brei, A.V. Melezhyk, S.V. Prudius, E.I. Oranskaya, Polish journal of chemistry 83(4) (2009) 537-546.

[31] B. M. Reddy, P. M. Sreekanth, Synthetic Communications, 32(18) (2002) 2815-2819.

[32] R. Sakthivel, H. Prescott, E. Kemnitz, Journal of Molecular Catalysis A: Chemical 223 (2004) 137–142.

[33] A. Bordoloi, N. T. Mathew, B. M. Devassy, S.P. Mirajkar, S.B. Halligudi, Journal of Molecular Catalysis A: Chemical 247 (2006) 58–64.

[34] S. Ramu, N. Lingaiah, B.L.A. Prabhavathi Devi, R.B.N. Prasad, I. Suryanarayana, P.S. Sai Prasad, Applied Catalysis A: General 276 (2004)163–168.

[35] D. E. López, K. Suwannakarn, D. A. Bruce, J. G. Goodwin Jr, Journal of Catalysis 247 (2007) 43–50.

[36] F. Figueras, J. Palomeque, S. Loridant, C. Fèche, N. Essayem, G. Gelbard, Journal of Catalysis, 226 (2004) 25-31.

[37] S. Loridant, C. Feche, N. Essayem, F. Figueras, J.Phys.Chem.B, 109(12) (2005) 5631.

[38] F. Chambon, F. Rataboul, C. Pinel, A. Cabiac, E. Guillon, N. Essayem, Applied Catalysis A: General, 504 (2015) 664–671.

[39] C. Nguyen, N. Q. Bui, M. Eternot, T.T.H. Vu, P. Fongarland, N. Essayem, J.Mol.Catal, 458 (2018) 171-179.

[40] X. Wang, J. Zhao, X. Hou, Q. He, C. Tang, Journal of Nanomaterials, 1 (2012) 1-5.

[41] E. Torres-García, A. Peláiz-Barranco, C. Vázquez-Ramos, G.A. Fuentes, J. Mater. Res., 8 (2001) 2209-2212.

[42] M. Aghazadeh, A-A. M. Barmi, M. Hosseinifard, Materials Letters 73 (2012) 28–31.

[43] E. Torres-García, G. Rosas, J. A. Ascencio, E. Haro-Poniatowski, R. Pérez, Appl. Phys. A, 79 (2004) 401–406.

[44] R.A. Nyquist, R.O. Kagel. Handbook of infrared and raman spectra of inorganic compound and organic salts, vol. 4. Tokyo: Academic press; 1997. p. 223.

[45] I. E. Wachs, T. Kim, E. I. Ross, Catalysis Today 116 (2006) 162–168.

[46] V. Jollet, F. Chambon, F. Rataboul, A. Cabiac, C. Pinel, E. Guillon, N. Essayem, Green Chem., 11 (2009) 2052–2060.

[47] X. Lei, F-F. Wang, C-L. Liu, R-Z Yang, W-S. Dong, *Applied Catalysis A: General*, 482 (2014) 78–83.

ZrW catalyzed cellulose conversion in hydrothermal conditions: Influence of the calcination temperature and insights on the nature of the active phase

Van Chuc NGUYEN[1,2], Amar DANDACH[1], Thi Thu Ha VU[2], Pascal FONGARLAND[1], Nadine ESSAYEM[1*]

[1]*Institut de Recherche sur la Catalyse et l'environnement de Lyon, CNRS, Lyon1, 2 Avenue Albert Einstein, 69626 Villeurbanne, France*

[2]*Key Laboratory for Petrochemical and Refinery Technologies, 2 rue Pham Ngu Lao, Hanoi, Vietnam*

* nadine.essayem@ircelyon.univ-lyon1.fr

We report here a comparison between calcined and un-calcined ZrW to that of zirconium oxyhydroxide and calcined zirconia in the hydrolysis of cellulose. The results stress that the active phase of the Zr based catalysts might combine the couple Zr^{4+} and OH^- species while the role of W species would be of secondary importance and contribute to enhance the overall acid strength and the amount of acid sites. Of prime importance, it is disclosed that un-calcined ZrW exhibits a higher stability than calcined ZrW against W leaching.

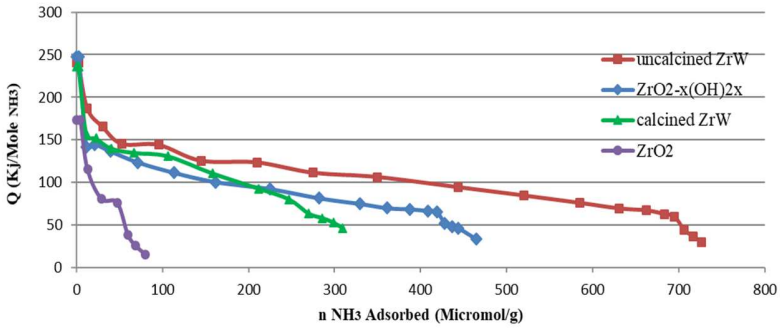

.